Supplementary Information

S1. Distinct switching rates in either direction

In this section, we investigate the system (5)-(7) subject to the phenotypic switching functions listed in Table S1 with different switching rates in either direction, such that cells in phenotypic state 1 switch to phenotypic state 2 at rate $s_{12} \in \mathbb{R}_+$ and, equivalently, cells in phenotypic state 2 switch to phenotypic state 1 at a rate given by $s_{21} \in \mathbb{R}_+$. Since there is limited evidence that distinctly different switching rates are biologically relevant [61], we only briefly discuss some of the main results for $s_{12} \neq s_{21}$ in this section to demonstrate these parameters' impact on the model solutions.

Name	$\gamma_{12}(u_1, u_2, m)$	$\gamma_{21}(u_1, u_2, m)$
Constant switching	s_{12}	s_{21}
ECM-dependent switching	$s_{12}(1-m)$	$s_{21}m$
Space-dependent switching	$s_{12}(1-u_1-u_2-m)$	$s_{21}(u_1+u_2+m)$
Cell-dependent switching	$s_{12}(1-u_1-u_2)$	$s_{21}(u_1+u_2)$

Table S1: Table listing the phenotypic switching functions.

Fig. S1 shows that, in the case of constant switching, the ratio between the phenotypic switching rates, s_{12} and s_{21}, directly determines the ratio between the volume fraction of cells in phenotypic states 1 and 2 in the bulk of the migrating cell population, as described in Appendix C.1. For s_{12}, $s_{21} \in [0, 1]$ the relationship between the travelling wave speed and these parameters is symmetrical around $s_{12} = s_{21}$, which is the maximum speed observed numerically and predicted analytically in the fast phenotypic switching regime (see Supplementary Material S2.3).

Furthermore, changes in the individual switching rates also impact the travelling wave profile and speed of migration. For example, when considering ECM-dependent switching, although increasing the switching rate from phenotypic state 2 to phenotypic state 1 decreases the travelling wave speed, it also changes the distribution of cells in the migrating front such that the front of the travelling wave is dominated by degrading cells in phenotypic state 1, ahead of a mixed region of cells in both states, and the bulk of proliferating cells remains in the rear (see Fig. S2).

A similar result can be observed in Fig. S2 for space-dependent switching and cell-dependent switching. In these cases, increasing the switching rate from phenotypic state 1 to phenotypic state 2 causes a leading population of cells in phenotypic state 2 at the front of the travelling wave. In all cases, the greater the difference between the switching rates, the larger and more concentrated this proportion of leader cells are.

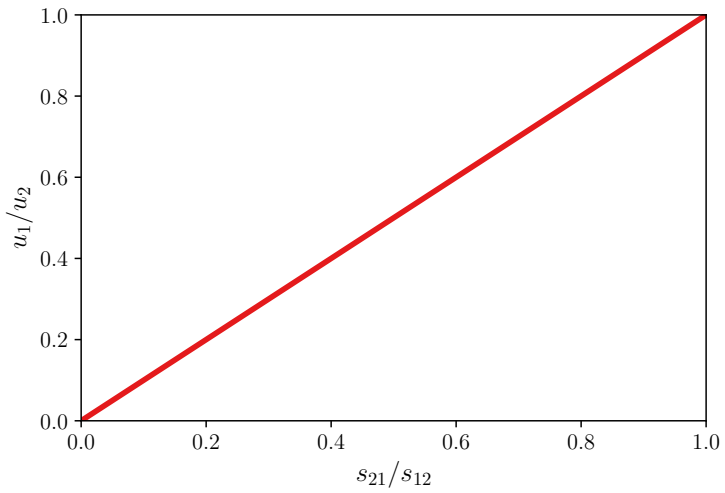

Figure S1: Plot demonstrating the relationship between the ratio of the switching rates, s_{12} and s_{21}, and the ratio between the volume fraction of the two cell sub-populations behind the wave front, u_1/u_2 when simulating the system (5)-(7) subject to the initial conditions for the cells as in Eq. (8), and for the ECM as in Eq. (4), subject to constant phenotypic switching (see Table 1). This plot was produced by running simulations under a variety of switching rates and plotting the ratio between the resulting cell sub-population densities behind the wave front. The initial ECM volume fraction ahead of the cells is $m_0 = 0.5$, the ECM degradation rate is $\lambda = 1$, and the width of the region initially invaded by migrating cells is $\alpha = 1$ across all simulations. For more information regarding the numerical methods used see Appendix D.

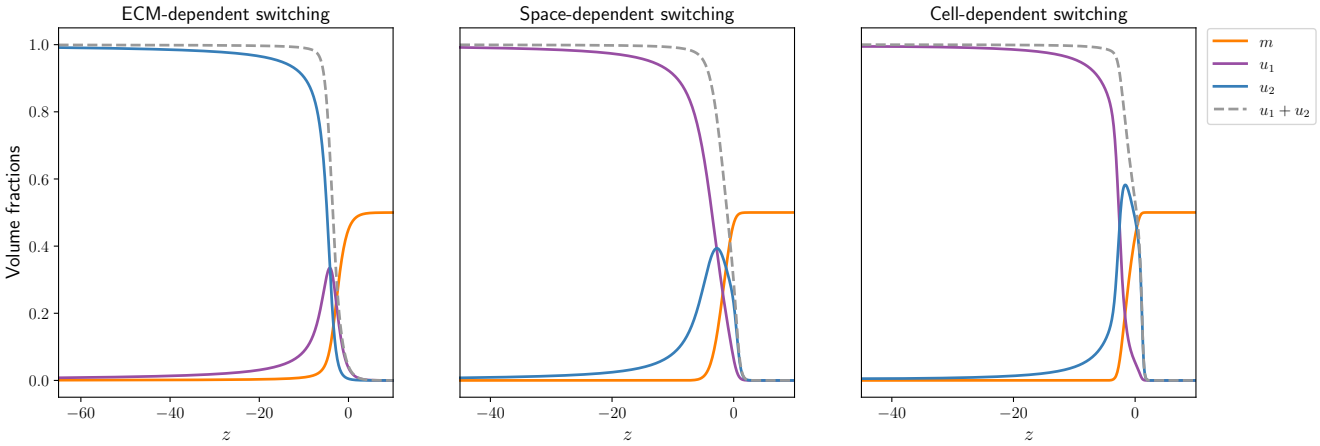

Figure S2: Travelling wave profiles of the solutions of Eqs. (5)-(7) subject to the initial conditions for the cells in Eq. (8), and for the ECM in Eq. (4), plotted as a function of the travelling wave variable $z = x - ct$, where c is the numerically observed travelling wave speed. These solutions demonstrate that changing the switching rate in one direction leads to one sub-population dominating the migrating front. For ECM-dependent switching, the switching rate from phenotypic state 1 to 2 is $s_{12} = 1$ and the switching rate from phenotypic state 2 to 1 is $s_{21} = 10$. For space- and cell-dependent switching, the switching rate from phenotypic state 1 to 2 is $s_{12} = 10$ and the switching rate from phenotypic state 2 to 1 is $s_{21} = 1$. The initial ECM volume fraction ahead of the cells is $m_0 = 0.5$, the ECM degradation rate is $\lambda = 1$, the weighting of the specialists towards degrading ECM is $\theta_{S,D} = 0.5$ and the width of the region initially invaded by migrating cells is $\alpha = 1$ in all cases. For more information regarding the numerical methods used see Appendix D.

S2. Formal travelling wave analysis in the fast phenotypic switching regime

In a regime where phenotypic switching is faster than cell motility and proliferation, we can consider the following rescaled model

$$\begin{aligned}
\frac{\partial u_{1_\epsilon}}{\partial t} &= (1-\theta_{S,D})\frac{\partial}{\partial x}\left[\left(1-u_{1_\epsilon}-u_{2_\epsilon}-m_\epsilon\right)\frac{\partial u_1}{\partial x}+u_{1_\epsilon}\frac{\partial}{\partial x}\left(u_{1_\epsilon}+u_{2_\epsilon}+m_\epsilon\right)\right] \\
&\qquad + \frac{1}{\epsilon}u_{2_\epsilon}\gamma_{21}(u_{1_\epsilon},u_{2_\epsilon},m_\epsilon) - \frac{1}{\epsilon}u_{1_\epsilon}\gamma_{12}(u_{1_\epsilon},u_{2_\epsilon},m_\epsilon), \\
\frac{\partial u_{2_\epsilon}}{\partial t} &= \theta_{S,P}u_{2_\epsilon}\left(1-u_{1_\epsilon}-u_{2_\epsilon}-m_\epsilon\right) \\
&\qquad - \frac{1}{\epsilon}u_{2_\epsilon}\gamma_{21}(u_{1_\epsilon},u_{2_\epsilon},m_\epsilon) + \frac{1}{\epsilon}u_{1_\epsilon}\gamma_{12}(u_{1_\epsilon},u_{2_\epsilon},m_\epsilon), \\
\frac{\partial m_\epsilon}{\partial t} &= -\theta_{S,D}\lambda m u_{1_\epsilon},
\end{aligned}$$

where $\epsilon \in \mathbb{R}_+$, $x \in \mathbb{R}$ and $t \in \mathbb{R}_+$. Here, $\lambda \in \mathbb{R}_+$ is the rescaled rate of ECM degradation by cells in phenotypic state 1, whilst $\theta_{S,D} \in [0,1]$ describes the weighting of cells in phenotypic state 1 towards degrading ECM, $\theta_{S,P} = 1$ describes the weighting of cells in phenotypic state 2 towards proliferation, and

$$\gamma_{12} : \mathbb{R}_+^3 \to \mathbb{R}_+ \qquad \text{and} \qquad \gamma_{21} : \mathbb{R}_+^3 \to \mathbb{R}_+,$$

are the non-dimensional phenotypic switching functions.

Simulations reveal that the model admits constant profile, constant speed travelling wave solutions, so we introduce the travelling wave ansatz

$$\begin{aligned}
U_{p_\epsilon}(z) &= U_{p_\epsilon}(x-ct) = u_{p_\epsilon}(x,t), \\
M_\epsilon(z) &= M_\epsilon(x-ct) \ = m_\epsilon(x,t),
\end{aligned}$$

for $p = \{1, 2\}$, where $c \in \mathbb{R}_+$, that satisfy the following system of ODEs:

$$\begin{aligned}
-c\frac{\mathrm{d}U_{1_\epsilon}}{\mathrm{d}z} &= (1-\theta_{S,D})\frac{\mathrm{d}}{\mathrm{d}z}\left[(1-U_{1_\epsilon}-U_{2_\epsilon}-M_\epsilon)\frac{\mathrm{d}U_{1_\epsilon}}{\mathrm{d}z}+U_{1_\epsilon}\frac{\mathrm{d}}{\mathrm{d}z}(U_{1_\epsilon}+U_{2_\epsilon}+M_\epsilon)\right] \\
&\qquad - \frac{1}{\epsilon}U_{1_\epsilon}\gamma_{12}(U_{1_\epsilon},U_{2_\epsilon},M_\epsilon) + \frac{1}{\epsilon}U_{2_\epsilon}\gamma_{21}(U_{1_\epsilon},U_{2_\epsilon},M_\epsilon), \qquad \text{(S1)} \\
-c\frac{\mathrm{d}U_{2_\epsilon}}{\mathrm{d}z} &= U_{2_\epsilon}(1-U_{1_\epsilon}-U_{2_\epsilon}-M_\epsilon) \\
&\qquad + \frac{1}{\epsilon}U_{1_\epsilon}\gamma_{12}(U_{1_\epsilon},U_{2_\epsilon},M_\epsilon) - \frac{1}{\epsilon}U_{2_\epsilon}\gamma_{21}(U_{1_\epsilon},U_{2_\epsilon},M_\epsilon), \qquad \text{(S2)} \\
-c\frac{\mathrm{d}M_\epsilon}{\mathrm{d}z} &= -\lambda\theta_{S,D}U_{1_\epsilon}M_\epsilon. \qquad \text{(S3)}
\end{aligned}$$

Combining Eqs. (S1) and (S2) we find that the total cell volume fraction

$$U_\epsilon(z) = U_{1_\epsilon}(z) + U_{2_\epsilon}(z),$$

satisfies the ODE

$$-c\frac{\mathrm{d}U_\epsilon}{\mathrm{d}z} = (1-\theta_{S,D})\frac{\mathrm{d}}{\mathrm{d}z}\left[(1-U_\epsilon-M_\epsilon)\frac{\mathrm{d}U_{1_\epsilon}}{\mathrm{d}z}+U_{1_\epsilon}\frac{\mathrm{d}}{\mathrm{d}z}(U_\epsilon+M_\epsilon)\right] + U_{2_\epsilon}(1-U_\epsilon-M_\epsilon), \qquad \text{(S4)}$$

for $z \in \mathbb{R}$.

Now consider constant phenotypic switching as defined in Table S1 and look for an analytical expression for the travelling wave speed in asymptotic regions of λ, following the ideas in [3].

By considering the asymptotic expansions around U_ϵ, U_{1_ϵ}, U_{2_ϵ} and M_ϵ such that the leading-order terms are given by U, U_1, U_2 and M, respectively, then as $\epsilon \to 0^+$ we formally find, from Eqs. (S1) and (S2), that

$$U_p(z) = \omega_p(U_1, U_2, M)U, \tag{S5}$$

where

$$\omega_1 = \frac{s_{21}}{s_{12} + s_{21}},$$
$$\omega_2 = \frac{s_{12}}{s_{12} + s_{21}}.$$

By substitution, Eq. (S4) becomes

$$-c\frac{\mathrm{d}U}{\mathrm{d}z} = \omega_1(1-\theta_{S,D})\frac{\mathrm{d}}{\mathrm{d}z}\left[(1-U-M)\frac{\mathrm{d}U}{\mathrm{d}z} + U\frac{\mathrm{d}}{\mathrm{d}z}(U+M)\right] + \omega_2 U(1-U-M),$$

which can be expanded and written as

$$\omega_1(1-\theta_{S,D})(1-M)\frac{\mathrm{d}^2U}{\mathrm{d}z^2} + c\frac{\mathrm{d}U}{\mathrm{d}z} + \omega_2 U(1-U-M) = -\omega_1(1-\theta_{S,D})U\frac{\mathrm{d}^2M}{\mathrm{d}z^2}. \tag{S6}$$

Furthermore, Eq. (S3) can be written as

$$c\frac{\mathrm{d}M}{\mathrm{d}z} = \lambda\theta_{S,D}\omega_1 UM, \tag{S7}$$

which yields

$$\begin{aligned}\frac{\mathrm{d}^2M}{\mathrm{d}z^2} &= \frac{\lambda\theta_{S,D}\omega_1}{c}\left(U\frac{\mathrm{d}M}{\mathrm{d}z} + M\frac{\mathrm{d}U}{\mathrm{d}z}\right)\\ &= \frac{\lambda\theta_{S,D}\omega_1}{c}\left(\frac{\lambda\theta_{S,D}\omega_1}{c}MU^2 + M\frac{\mathrm{d}U}{\mathrm{d}z}\right).\end{aligned} \tag{S8}$$

Substituting Eq. (S8) into Eq. (S6) we find

$$\begin{aligned}&\omega_1(1-\theta_{S,D})(1-M)\frac{\mathrm{d}^2U}{\mathrm{d}z^2} + c\frac{\mathrm{d}U}{\mathrm{d}z} + \omega_2 U(1-U-M)\\ &\quad = -\frac{\lambda\theta_{S,D}\omega_1^2(1-\theta_{S,D})}{c}MU\left[\frac{\lambda\theta_{S,D}\omega_1}{c}U^2 + \frac{\mathrm{d}U}{\mathrm{d}z}\right].\end{aligned} \tag{S9}$$

Moreover, solving Eq. (S7) subject to the boundary condition $M(z) \to m_0$ as $z \to \infty$, where $m_0 \in [0,1]$, gives

$$M(z) = m_0\exp\left\{-\frac{\lambda\theta_{S,D}\omega_1}{c}\int_z^\infty U(s)\mathrm{d}s\right\}. \tag{S10}$$

Under the boundary conditions $U_p(z) \to 0$ as $z \to \infty$ for $p = 1, 2$ we have $U(z) \to 0$ as $z \to \infty$. At the migrating front of the travelling wave (i.e., for $z \in (\ell, \infty)$ with $1 \ll \ell < \infty$), we can use the ansatz

$$U(z) \approx \exp\{-\beta z\},$$

where $\beta \in (0, \infty)$ to give

$$M(z) = m_0\exp\left\{-\frac{\lambda\theta_{S,D}\omega_1}{\beta c}U(z)\right\}, \tag{S11}$$

for $z \in (\ell, \infty)$.

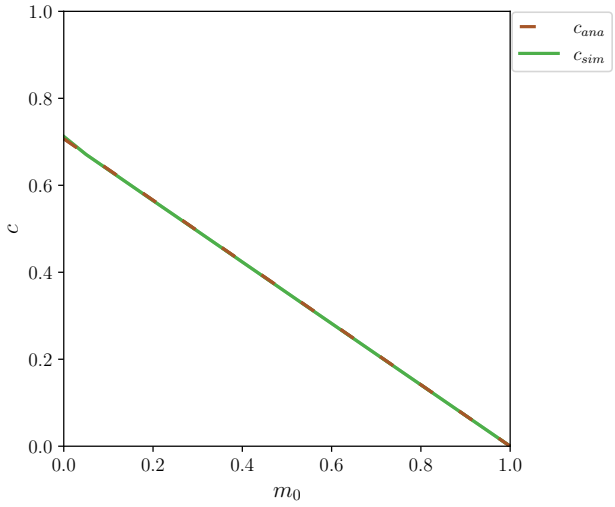

Figure S3: Plot showing the analytically predicted minimum travelling wave speed, c_{ana}, and the numerically estimated travelling wave speed, c_{sim}, of solutions of the system (5)-(7) subject to the initial conditions for the cells as in Eq. (8), and for the ECM as in Eq. (4) for very low ECM degradation rates, $\lambda \to 0^+$, and various initial ECM volume fractions ahead of the cells, m_0, in fast phenotypic switching regimes, defined by simulations with $s_{12} = s_{21} = s = 10^4$. The numerically estimated travelling wave speeds plotted in green are for simulations with $\lambda \leq 10^{-2}$, while the analytical wave speeds plotted in red are given by Eq. (S15). The width of the region initially invaded by migrating cells is $\alpha = 1$ and the weighting of specialists towards degradation is $\theta_{S,D} = 0.5$ across all simulations. For more information regarding the numerical methods used see Appendix D.

S2.1. Formal asymptotic analysis for $\lambda \to 0^+$

Using Eq. (S11), it is clear that

$$M(z) \approx m_0 \exp\left\{ -\frac{\lambda \theta_{S,D} \omega_1}{\beta c} U(z) \right\} \to m_0 \qquad \text{as} \qquad \lambda \to 0^+, \tag{S12}$$

for $z \in (\ell, \infty)$. In the asymptotic regime $\lambda \to 0^+$, since $0 < U(z) < 1$ and $\mathrm{d}U(z)/\mathrm{d}z \approx -\beta U(z)$ for $z \in (\ell, \infty)$, substituting Eq. (S12) into Eq. (S9) results in the asymptotic relation

$$U(z) m_0 \exp\left\{ -\frac{\lambda \theta_{S,D} \omega_1}{\beta c} U(z) \right\} \left[\frac{\lambda \theta_{S,D} \omega_1}{c} U^2(z) + \frac{\mathrm{d}U(z)}{\mathrm{d}z} \right] \to 0 \qquad \text{as} \qquad \lambda \to 0^+,$$

for $z \in (\ell, \infty)$. Formally, we find

$$\omega_1 (1 - \theta_{S,D})(1 - M) \frac{\mathrm{d}^2 U}{\mathrm{d}z^2} + c \frac{\mathrm{d}U}{\mathrm{d}z} + \omega_2 U (1 - U - M) \approx 0, \tag{S13}$$

for $z \in (\ell, \infty)$. We notice that Eq. (S13) is equivalent to the Fisher-KPP model [9, 10] in travelling-wave co-ordinates:

$$\tilde{D} \frac{\mathrm{d}^2 \tilde{U}(z)}{\mathrm{d}z^2} + \tilde{c} \frac{\mathrm{d}\tilde{U}}{\mathrm{d}z} + \tilde{r} \tilde{U} \left(1 - \frac{\tilde{U}}{\tilde{K}} \right) = 0, \tag{S14}$$

where we have $\tilde{D} = \omega_1 (1 - \theta_{S,D})(1 - m_0)$, $\tilde{r} = \omega_2 (1 - m_0)$ and $\tilde{K} = (1 - m_0)$. This correctly predicts (see Fig. S3), as $\lambda \to 0^+$, a minimum travelling wave speed given by

$$c_{\min} = 2(1 - m_0) \sqrt{\omega_1 \omega_2 (1 - \theta_{S,D})}, \tag{S15}$$

which can be observed in Fig. S3 to agree with the numerically estimated wave speed for the system (5)-(7) when $\lambda \to 0^+$.

S2.2. Formal asymptotic analysis for $\lambda \to \infty$

Revisiting the semi-explicit solution for M given by Eq. (S11), we find

$$M(z) \approx m_0 \exp\left\{ -\frac{\lambda \theta_{S,D} \omega_1}{\beta c} U(z) \right\} \to 0 \qquad \text{as} \qquad \lambda \to \infty, \tag{S16}$$

for $z \in (\ell, \infty)$. In the asymptotic regime $\lambda \to \infty$, since $0 < U(z) < 1$ and $\mathrm{d}U(z)/\mathrm{d}z \approx -\beta U(z)$ for $z \in (\ell, \infty)$, substituting Eq. (S16) into Eq. (S6) results in the asymptotic relation

$$U(z) m_0 \exp\left\{ -\frac{\lambda \theta_{S,D} \omega_1}{\beta c} U(z) \right\} \left[\frac{\lambda \theta_{S,D} \omega_1}{c} U^2(z) + \frac{\mathrm{d}U(z)}{\mathrm{d}z} \right] \to 0 \qquad \text{as} \qquad \lambda \to \infty,$$

for $z \in (\ell, \infty)$. By substitution, we then find

$$\omega_1 (1 - \theta_{S,D}) \frac{\mathrm{d}^2 U}{\mathrm{d}z^2} + c \frac{\mathrm{d}U}{\mathrm{d}z} + \omega_2 U (1 - U) \approx 0, \tag{S17}$$

for $z \in (\ell, \infty)$. In this case, Eq. (S17) is equivalent to the Fisher-KPP model (see Eq. (S14)) with parameters $\tilde{D} = \omega_1 (1 - \theta_{S,D})$, $\tilde{r} = \omega_2$ and $\tilde{K} = 1$, so when $\lambda \to \infty$ we have

$$c_{\min} = 2\sqrt{\omega_1 \omega_2 (1 - \theta_{S,D})}. \tag{S18}$$

Fig. S4 shows the convergence of the solutions to the system (5)-(7) to the solution of the Fisher-KPP model (see Eq. (S14)) with parameters $\tilde{D} = \omega_1 (1 - \theta_{S,D})$, $\tilde{r} = \omega_2$ and $\tilde{K} = 1$ as $\lambda \to \infty$.

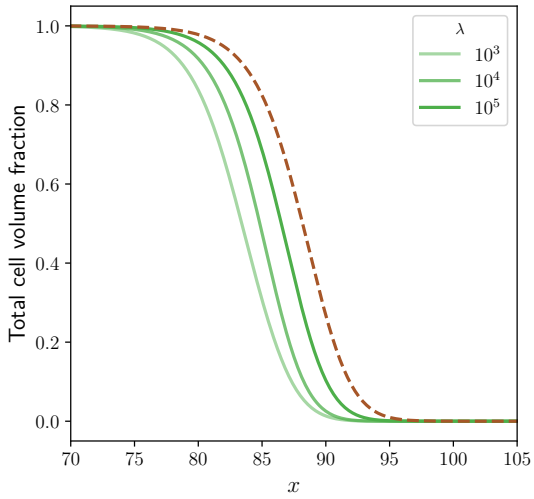

Figure S4: Plot of the total cell volume fraction obtained through numerical simulations of Eqs. (5)-(7) with constant phenotypic switching (see Table 1) subject to the initial conditions for the cells as in Eq. (8) and for the ECM as in Eq. (4) for large values of λ (solid lines), and numerical simulations of the Fisher-KPP model given by Eq. (S17) (dashed red line). In all simulations, solutions are shown at $t = 100$ and the initial ECM volume fraction ahead of the cells is $m_0 = 0.1$. The width of the region initially invaded by migrating cells is $\alpha = 1$, the weighting of specialists towards degradation is $\theta_{S,D} = 0.1$ and the switching rate for all functions is $s = \lambda$. Qualitatively, the same behaviour is observed for all $m_0 \in [0, 1)$. For more information regarding the numerical methods used see Appendix D.

S2.3. Maximising the travelling wave speed

In both $\lambda \to 0^+$ and $\lambda \to \infty$ regimes, the travelling wave speeds, determined by Eq. (S15) and Eq. (S18), respectively, are maximised when $\omega_1\omega_2$ is maximised. By considering

$$\omega_1\omega_2 = \frac{s_{12}s_{21}}{(s_{12}+s_{21})^2}, \tag{S19}$$

and differentiating twice with respect to s_{12}, it is clear that

$$\max(\omega_1\omega_2) = 0.25, \tag{S20}$$

which is obtained when $s_{12} = s_{21}$. As such, we can conclude that the travelling wave speed is always maximised when phenotypic switching between states 1 and 2 occurs at the same rate in either direction.